Int. J. Heat Mass Transfer. Vol. 30, No. 6, pp. 1061–1075, 1987
Printed in Great Britain

0017-9310/87 $3.00+0.00

Free convection heat and mass transfer during pool penetration into a melting miscible substrate

F. B. CHEUNG
Department of Mechanical Engineering, Pennsylvania State University, University Park, PA 16802, U.S.A.

(*Received* 14 *July* 1986 *and in revised form* 19 *September* 1986)

Abstract—A theoretical investigation is made of the process of free convection melting of a solid slab by an overlying hot liquid pool. The solid, when molten, is lighter than and miscible with the pool material. Systematic mathematical approximations to the Boussinesq equations of motion are performed to determine the behavior of the temperature and the concentration fields in two different flow regions. These are the boundary layer region at the melting interface and the turbulent core region in the bulk pool. The dependence of the melting rate on various controlling parameters, including the Grashof number based on the pool-to-substrate density ratio, the external Stefan number based on the pool-to-substrate temperature difference, and the internal Stefan number based on the freezing-point depression, is obtained by matching the boundary layer solution and the turbulent core solution in the region of overlap. Comparison of the present theory is made with existing experiments and found to be good.

1. INTRODUCTION

THIS paper deals with the process of downward penetration of a horizontal solid substrate by an overlying hot liquid pool, a problem that has received considerable attention in the area of decay heat removal in nuclear reactors. The situation arises following a postulated severe core meltdown accident in a nuclear reactor when a layer of molten fuel or fuel–steel mixture comes in contact with the horizontal surface of a sacrificial bed. The sacrificial bed material, when molten, is miscible with and lighter than the core melt. Thus, the rate of melting is strongly dependent upon the motion of free convection in the melt layer driven by the density difference between the core melt and the molten sacrificial bed material. Understanding of the mechanism of the free convection melting process is essential to the design of a core-retention system.

A rather large number of studies have been performed on melting of solids in free convection flows, as can be seen in several recent review articles [1–3]. Most of these studies, however, have been motivated by the need to gain an understanding of heat transport in latent-heat-of-fusion energy storage systems where the melting solid and the liquid are of the same materials [4–10]. As such, the motion-driving buoyancy force is simply due to the variation of liquid density with temperature. In the problem under consideration here, the situation is quite different since the solid and the liquid are of different materials. The free convection motion is driven primarily by the sharp concentration or density gradient near the solid–liquid interface produced by melting of the solid. As a result, the melting rate not only depends on the temperature difference across the liquid layer, but also is a strong function of the density difference between the liquid and the substrate. Thus the present work falls into the category of double-diffusive convection [11, 12].

The first study of the melting and the associated convective motions in a heated liquid pool above a melting miscible substrate was performed by Farhadieh and Baker [13]. They used water soluble wax (polyethylene glycol) as the solid material and an aqueous salt solution heated by a suspending planar heater as the overlying pool to conduct the exploratory experiment. Various values of $(\Delta\rho/\rho_m)$, where $\Delta\rho$ is the difference between the bulk pool density, ρ_0, and the melt density, ρ_m, were employed in their experiments by changing the salt concentration in the liquid pool. A sharp concentration boundary layer was observed to exist near the solid–liquid melting interface. Extending from discrete sites of these boundary layers into the overlying heavier solution were melt fingers that injected melt materials into the liquid pool. The melt fingers lost their identities in the turbulent core region as a result of the intensive mixing motions there. This flow behavior is, in fact, quite similar to those observed in turbulent thermal convection in a horizontal fluid layer above a heated surface where the major resistance to heat transfer is contained in a thin boundary layer at the surface from which plumes of hot fluid or 'thermals' are generated [14, 15]. The heat transfer properties of this class of instability-driven flows have been determined experimentally in the absence of phase change for horizontal fluid layers heated from below [16–18], heated from within [19, 20], and with combined internal and external heating [21, 22].

In the range of $0.08 < \Delta\rho/\rho_m < 0.25$, Farhadieh and Baker [13] found that the melting rate, V_s, varied with the density ratio according to $V_s \sim (\Delta\rho/\rho_m)^{1/3}$, which was consistent with a pool flow regime for ordinary turbulent convection. For $\Delta\rho/\rho_m > 0.25$, however, the melting rate was observed to vary

NOMENCLATURE

A_0 integration constant, equation (43)
A_1 integration factor, dependent of Pr and Sc, equation (45a)
A_2 integration factor, independent of Pr and Sc, equation (45b)
B_0 integration constant, equation (44)
B_1 integration factor, dependent of Pr and Sc, equation (46a)
B_2 integration factor, independent of Pr and Sc, equation (46b)
C concentration
$\bar{C}$ mean concentration
$\bar{C}_c$ mean concentration profile in the turbulent core region, equation (38)
C_i mean concentration at the melting interface
C_0 bulk pool concentration
C_p specific heat
$\bar{C}_\delta$ mean concentration profile in the boundary layer region, equation (28)
ΔC_δ concentration difference across the boundary layer region
D mass diffusivity
f_1 boundary layer temperature function, equation (45a)
f_2 boundary layer concentration function, equation (46a)
g acceleration due to gravity
g_1 turbulent-core temperature function, equation (45b)
g_2 turbulent-core concentration function, equation (46b)
Gr modified Grashof number, equation (16)
k thermal conductivity
$\mathbf{k}$ unit vector in the vertical direction
L pool depth
m slope of the T–C freezing curve
P pressure
$\bar{P}$ mean pressure
p fluctuating pressure
Pr Prandtl number, ν/α
Re_m Reynolds number of the melting-induced flow, VL/ν
S location of the melting interface with respect to the non-moving frame
Sc Schmidt number, ν/D
Ste external Stefan number based on ΔT
Ste_d internal Stefan number based on ΔT_d
t time
T temperature
$\bar{T}$ mean temperature
$\bar{T}_c$ mean temperature profile in the turbulent-core region, equation (37)
T_d depressed freezing point at C_0
T_i mean temperature at the melting interface
T_{mp} normal freezing point
T_0 bulk pool temperature
$\bar{T}_\delta$ mean temperature profile in the boundary layer region, equation (27)
ΔT temperature difference between the bulk pool and the normal melting point of the substrate, $T_0 - T_{mp}$
ΔT_c temperature drop across the turbulent core region
ΔT_d freezing point depression at C_0, i.e. $\Delta T_d = T_{mp} - T_d$
ΔT_δ temperature drop across the boundary layer region
$\mathbf{u}$ velocity vector
V mean velocity component in the vertical direction at the melting interface with respect to the moving frame, equation (15)
V_s substrate-penetration rate
w vertical component of the fluctuating velocity
Y higher order quantity defined by equation (57)
z vertical coordinate in the moving frame
Z higher order quantity defined by equation (58).

Greek symbols

α thermal diffusivity
β isobaric coefficient of thermal expansion
γ coefficient of solute expansion, equation (12)
δ boundary layer thickness
η dimensionless boundary-layer coordinate, z/δ
θ fluctuating temperature
λ_s heat of fusion of the solid substrate
ν kinematic viscosity
ξ dimensionless turbulent-core coordinate, z/L
ρ liquid density
ρ_i liquid density at the melting interface
ρ_m density of the molten substrate, $\rho_0(1 - \gamma C_0)$
ρ_0 bulk pool density

ρ_s density of the solid substrate
$\Delta\rho$ density difference between the bulk solution pool and the molten substrate, $\rho_0 - \rho_m$.

Subscripts
0 bulk-pool conditions
c turbulent-core conditions
d freezing point depression
i melting interface
m molten substrate; moving coordinates
s solid substrate
δ boundary layer conditions.

Superscripts
$\bar{}$ mean quantities.

Other symbols
$\langle\ \rangle$ r.m.s. value of the fluctuating quantities.

according to $V_s \sim (\Delta\rho/\rho_m)^{4/3}$. They postulated that this sudden increase in the slope of the melting curve was due to a very vigorous turbulent flow regime, labeled as 'upper turbulent'. Within this regime, the melting rate was found to increase sharply with the pool-to-substrate temperature difference according to $V_s \sim \Delta T^{1.6}$.

Similar studies were made later on by Catton *et al.* [23], Eck and Werle [24], Fang *et al.* [25], and Epstein and Grolmes [26]. Catton *et al.* [23] used frozen benzene as the solid substrate and carbon tetrachloride or diiodomethane as the liquid pool material to yield high density ratios in the range of $0.72 < \Delta\rho/\rho_m < 2.26$. They found that the melting rate was very sensitive to the variation of the density ratio as reported by Farhadieh and Baker [13]. However, over the range of experimental conditions explored in their work, the melting rate was independent of the pool-to-substrate temperature difference.

Eck and Werle [24] conducted a series of experiments similar to those of Farhadieh and Baker [13] by using the same working material with the difference that the grid heater was replaced by a flat plate. They also observed an abrupt increase in the slope of the melting curve in the so-called upper turbulent regime, although large quantitative discrepancies in the measured melting rate were observed. The melting rate was found to be a linear function of ΔT rather than varying with $\Delta T^{1.6}$. Eck and Werle [24] attributed these discrepancies to the differences in the set-up of heater and thermal conductivities of test-section materials.

In an attempt to investigate the melting behavior in various flow regimes, Fang *et al.* [25] performed an experimental study of free convection melting of ice in aqueous salt solutions. The solid–liquid interface morphology, the free convection flow pattern near the moving phase boundary, and the corresponding ice melting rate were observed at different density ratios. Their results indicated that there was no upper turbulent regime as postulated by Farhadieh and Baker [13]. The measured ice melting rate simply varied according to the 1/3-power law in the entire turbulent flow region. Furthermore, the ice melting rate was almost independent of the pool-to-substrate temperature difference, as reported by Catton *et al.* [23]. It should be noted that the values of ΔT employed by Fang *et al.* [25] were rather small, with a typical value of 15°C.

Recently, Epstein and Grolmes [26] conducted an extensive laboratory study of the free convection melting problem using various pool–substrate material pairs: KI salt solution overlying frozen polyethylene glycol (PEG) and ice, $ZnBr_2$ salt solution overlying frozen glycerol and ice, and CCl_4 overlying frozen benzene. They uncovered an unexpected strong effect of the initial solid PEG temperature on the melting rate. The unconventional melting trends observed by Farhadieh and Baker [13] and Eck and Werle [24] were evidently not due to an abrupt change in the turbulent flow regime but rather due to the unexpected properties of this polymer material. By carefully controlling the initial PEG temperature, Epstein and Grolmes [26] were able to eliminate the sudden rise in the slope of the melting curve. The melting rate was found to vary according to $V_s \sim (\Delta\rho/\rho_m)^{1/3}$ at high density ratios, consistent with ordinary turbulent convection flow. This confirmed the experimental observation of Fang *et al.* [25] that the upper turbulent regime does not exist physically. Epstein and Grolmes [26] also examined the effect of ΔT on the melting rate over a wide range of pool-to-substrate temperature difference for various material pairs. Their results showed that the melting rate was a linear function of ΔT.

From the above review, it is evident that $V_s \sim (\Delta\rho/\rho_m)^{1/3}$ in the turbulent flow regime. However, the contradictory findings regarding the dependence of the melting rate on the pool-to-substrate temperature difference have yet to be resolved. So far, there is no physical explanation of observed melting behavior over the range of experimental conditions explored in laboratories. In addition, it is not known whether there are other important parameters that would strongly affect the free convection melting process. It is, therefore, highly desired to develop a

sound physical model based on the conservation laws to (i) describe the physical process of downward pool penetration, (ii) identify the appropriate controlling parameters, (iii) determine qualitatively and quantitatively the effects of these parameters, and (iv) explain the various experimental observations, particularly the data on the V_s–ΔT relation. These provide the major motivations for the present study.

2. THEORETICAL FORMULATION

Consider the process of downward penetration of a horizontal solid substrate by an overlying hot solution pool. The substrate, when molten, is miscible with and lighter than the solution. Because of the density difference between the substrate and the solution, instability-driven free convection flow occurs in the pool as melting proceeds. Both the density difference and the depth of the pool are assumed to be large such that the flow is turbulent. On the other hand, the total penetration distance is small compared to the depth of the pool so that the bulk pool concentration, C_0, and the corresponding bulk pool density, ρ_0, can be treated as constants during the free convection melting process. Assuming the fluid to be incompressible and its properties to be constant except density variation in the buoyancy force, the equations governing the convective motions are

$$\nabla\cdot\mathbf{u} = 0 \tag{1}$$

$$(\partial/\partial t - \nu\nabla^2)\mathbf{u} = -(\mathbf{u}\cdot\nabla)\mathbf{u} - \rho_0^{-1}\nabla p - \mathbf{k}g(\rho/\rho_0) \tag{2}$$

$$(\partial/\partial t - \alpha\nabla^2)T = -(\mathbf{u}\cdot\nabla)T \tag{3}$$

$$(\partial/\partial t - D\nabla^2)C = -(\mathbf{u}\cdot\nabla)C. \tag{4}$$

For the case of small total penetration distance relative to the depth of the pool, laboratory observations [13, 23–26] show that the melting rate and the mean quantities are essentially steady and one-dimensional. Thus, we may transform the above equations to a moving coordinate system fixed to the solution pool–solid substrate interface to remove the time dependence of the mean quantities. With the interface position given as $z_i = S(t)$, we write

$$z = z_m + S(t) \quad \text{and} \quad w = w_m + \frac{dS}{dt} \tag{5}$$

where z_m and w_m are the vertical coordinate and the vertical velocity component in the moving frame, respectively. Decomposing the dependent variable into the mean and fluctuating parts, we have

$$T = \bar{T} + \theta, \quad \bar{T} = \bar{T}(z_m), \quad \bar{\theta} = 0 \tag{6a}$$

$$C = \bar{C} + \phi, \quad \bar{C} = \bar{C}(z_m), \quad \bar{\phi} = 0 \tag{6b}$$

$$V_s = -\frac{dS}{dt}, \quad \bar{\mathbf{u}}_m = 0. \tag{6c}$$

With the substitution of equations (5) and (6) into equations (1)–(4) the governing equations with the subscript m dropped for clarity become

$$\alpha\frac{d^2\bar{T}}{dz^2} - \frac{d}{dz}\overline{w\theta} = 0 \tag{7}$$

$$D\frac{d^2\bar{C}}{dz^2} - \frac{d}{dz}\overline{w\phi} = 0 \tag{8}$$

$$(\partial/\partial t - \nu\nabla^2)\mathbf{u} = -(\mathbf{u}\cdot\nabla)u - \rho_0^{-1}\nabla p + \mathbf{k}g\gamma\phi \tag{9}$$

$$(\partial/\partial t - \alpha\nabla^2)\theta = -w\frac{d\bar{T}}{dz} - [(\mathbf{u}\cdot\nabla)\theta - \overline{(\mathbf{u}\cdot\nabla)\theta}] \tag{10}$$

$$(\partial/\partial t - D\nabla^2)\phi = -w\frac{d\bar{C}}{dz} - [(\mathbf{u}\cdot\nabla)\phi - \overline{(\mathbf{u}\cdot\nabla)\phi}] \tag{11}$$

where $p = P - \bar{P} - \rho_0\overline{w^2}$ is the fluctuating pressure and γ is the coefficient of solute expansion given by

$$\gamma = \frac{1}{\rho}\frac{\partial\rho}{\partial C} = \frac{1}{\rho_0}\frac{\rho_0 - \rho}{C_0 - C}. \tag{12}$$

In writing equation (9), we have assumed the density difference between the substrate and the solution to be sufficiently large so that the effect of thermal expansion can be ignored. Mathematically, this requires $\gamma\Delta C \gg \beta\Delta T$, which has been satisfied in all the experiments [13, 23–26] discussed in the previous section.

The boundary conditions for the above system of equations can be derived from the no-slip condition, the freezing curve, and the conservation of mass, heat, and solute. In the bulk solution pool, i.e. $z \sim L$, we have

$$\bar{T} = T_0, \quad \bar{C} = C_0, \quad \bar{\rho} = \rho_0 \tag{13}$$

where T_0 and C_0 are given quantities and $\rho_0 = \rho_0(C_0)$. At the melting interface, i.e. $z = 0$, we have

$$\overline{w\theta} = \overline{w\phi} = 0, \quad \bar{T} = T_i, \quad \bar{C} = C_i \tag{14a}$$

$$T_{mp} - T_i = mC_i \tag{14b}$$

$$k\frac{d\bar{T}}{dz} = \rho_i\lambda_s V \quad \text{or} \quad \alpha\frac{d\bar{T}}{dz} = \frac{\lambda_s}{C_p}V \tag{14c}$$

$$D\frac{d\bar{C}}{dz} = \frac{\rho_s}{\rho_i}V_sC_i = VC_i \tag{14d}$$

where V is the mean vertical velocity at the moving interface given by

$$V = -\frac{\rho_s}{\rho_i}\frac{dS}{dt} = \frac{\rho_s}{\rho_i}V_s. \tag{15}$$

In writing equation (14b), the freezing curve has been approximated by a straight line with the slope equal to m. Equations (14c) and (14d) represent the heat flux and solute flux conditions at the interface, respectively. The initial substrate temperature is assumed to be at its melting point. Note that $\rho_i = \rho_i(C_i)$ and T_i, C_i, and V are unknown quantities to be determined during the course of analysis.

Equations (7) and (8) may be integrated once using the boundary conditions at the interface to yield

$$\alpha\frac{d\bar{T}}{dz}-\overline{w\theta}=\frac{\lambda_s}{C_p}V \tag{16}$$

and

$$D\frac{d\bar{C}}{dz}-\overline{w\phi}=VC_i. \tag{17}$$

The goal is to determine the dimensionless melting rate or the melting-induced Reynolds number, $Re_m = VL/\nu$, as a function of the Prandtl number, $Pr = \nu/\alpha$, the Schmidt number, $Sc = \nu/D$, the external Stefan number based on the pool-to-substrate temperature difference, $Ste = C_p(T_0 - T_{mp})/\lambda_s$, the internal Stefan number based on the freezing point depression, $Ste_d = C_p(T_{mp} - T_d)/\lambda_p$, where T_d is the freezing temperature of the bulk solution at C_0 (i.e. $T_d = T_{mp} - mC_0$), and the modified Grashof number

$$Gr=\frac{g(\Delta\rho/\rho_0)L^3}{\nu^2}=\frac{g\gamma C_0L^3}{\nu^2} \tag{18}$$

where the last expression of the above equation has been derived from equation (12) with $\Delta\rho = \rho_0 - \rho_m$ and $\rho_m = \rho(C = 0) = \rho_0(1 - \gamma C_0)$. Note that C_0 actually represents the concentration differences between the bulk solution pool and the pure molten substrate.

3. ANALYSIS

We consider the case of moderate Prandtl and Schmidt numbers where the velocity, thermal, and concentration boundary layers have about the same thickness. In what follows, we seek the temperature and the concentration behaviors in two principal flow regions of the solution pool. These are the boundary layer region where $0 < z < \delta$ and the turbulent core region where $\delta < z < L$. The functional dependence of Re_m on Gr, Ste, and Ste_d will be determined by matching of the boundary layer and the turbulent core solutions in the region of overlap.

3.1. *Boundary layer region* ($0 < z < \delta$)

In this region, the wall effect is strong. We may assume that molecular transport dominates the corresponding eddy transport. Equations (16) and (17) may be approximated by

$$\left|\alpha\frac{d\bar{T}}{dz}\right|\sim\left|\frac{\lambda_s}{C_p}V\right| \quad\text{or}\quad \alpha\frac{\Delta T_\delta}{\delta}\sim\frac{\lambda_s}{C_p}V \tag{19}$$

and

$$\left|D\frac{d\bar{C}}{dz}\right|\sim|VC_i| \quad\text{or}\quad D\frac{\Delta C_\delta}{\delta}\sim VC_i \tag{20}$$

where ΔT_δ and ΔC_δ are the temperature and the concentration drops across the boundary layer, respectively. In addition, we may ignore the advection term relative to the viscous term in the wall region. Thus, a balance between the viscous term and the buoyancy term in equation (9) gives

$$|\nu\nabla^2\mathbf{u}|\sim|g\gamma\phi|$$
$$\text{or}\quad \nu\frac{\langle w\rangle_\delta}{\delta^2}\sim g\gamma\langle\phi\rangle_\delta \tag{21}$$

where $\langle\ \rangle$ denotes the r.m.s. values and the subscript δ refers to the boundary layer. Similarly, from equations (10) and (11), we have

$$|\alpha\nabla^2\theta|\sim\left|w\frac{d\bar{T}}{dz}\right| \quad\text{or}\quad \alpha\frac{\langle\theta\rangle_\delta}{\delta^2}\sim\langle w\rangle_\delta\frac{\Delta T_\delta}{\delta} \tag{22}$$

and

$$|D\nabla^2\phi|\sim\left|w\frac{d\bar{C}}{dz}\right| \quad\text{or}\quad D\frac{\langle\phi\rangle_\delta}{\delta^2}\sim\langle w\rangle_\delta\frac{\Delta C_\delta}{\delta}. \tag{23}$$

Equations (19)–(23) lead to

$$\frac{\delta}{L}\sim\left[Gr\,Re_m\,Sc^2\left(\frac{C_i}{C_0}\right)\right]^{-1/4} \tag{24}$$

$$\Delta T_\delta\sim\frac{\lambda_s}{C_p}Pr\left[Gr\,Re_m^{-3}\,Sc^2\left(\frac{C_i}{C_0}\right)\right]^{-1/4} \tag{25}$$

and

$$\Delta C_\delta\sim\left[Gr\,Re_m^{-3}\,Sc^{-2}\left(\frac{C_i}{C_0}\right)^{-3}\right]^{-1/4}C_0. \tag{26}$$

From equations (25) and (26), we may construct the near-field temperature and concentration profiles, $\bar{T}_\delta$ and $\bar{C}_\delta$, respectively, in the boundary layer region as follows:

$$\bar{T}_\delta = T_i+\frac{\lambda_s}{C_p}Pr\left[Gr\,Re_m^{-3}\,Sc^2\left(\frac{C_i}{C_0}\right)\right]^{-1/4}f_1(\eta) \tag{27}$$

and

$$\bar{C}_\delta = C_i+\left[Gr\,Re_m^{-3}\,Sc^{-2}\left(\frac{C_i}{C_0}\right)^{-3}\right]^{-1/4}C_0f_2(\eta) \tag{28}$$

where f_1 and f_2 are unknown functions of η to be determined in the course of analysis and $\eta = z/\delta$ is the dimensionless boundary layer coordinate. Since molecular transport is important in the flow region, both f_1 and f_2 can be functions of the Prandtl number and the Schmidt number of the fluid.

3.2. *Turbulent core region* ($\delta < z < L$)

In this region, the wall effect is not important. We may assume that eddy transport dominates over the corresponding molecular transport. Equations (16)

and (17) may be approximated by

$$|\overline{w\theta}| \sim \left|\frac{\lambda_s}{C_p} V\right| \quad \text{or} \quad \langle w\rangle_c\langle\theta\rangle_c \sim \frac{\lambda_s}{C_p} V \tag{29}$$

and

$$|\overline{w\phi}| \sim |VC_i| \quad \text{or} \quad \langle w\rangle_c\langle\phi\rangle_c \sim VC_s \tag{30}$$

where the subscript c refers to the turbulent core. In addition, we may ignore the viscous term relative to the advection term in the bulk pool region. Thus, a balance between the advection term and the buoyancy term in equation (9) gives

$$|(\mathbf{u}\cdot\nabla)\mathbf{u}| \sim |g\gamma\phi| \quad \text{or} \quad \langle w\rangle_c^2/L \sim g\gamma\langle\phi\rangle_c \tag{31}$$

where a length scale of mixing equal to the pool depth has been used in the above equation. Similarly, from equations (10) and (11), we have

$$|(\mathbf{u}\cdot\nabla)\theta| \sim \left|w\frac{d\bar{T}}{dz}\right| \quad \text{or} \quad \Delta T_c \sim \langle\theta\rangle_c \tag{32}$$

and

$$|(\mathbf{u}\cdot\nabla)\phi| \sim \left|w\frac{d\bar{C}}{dz}\right| \quad \text{or} \quad \Delta C_c \sim \langle\phi\rangle_c \tag{33}$$

where ΔT_c and ΔC_c are the temperature and concentration differences across the turbulent core region, respectively. Equations (32) and (33) imply that the values of ΔT_c and ΔC_c, being the same order as the fluctuating quantities, are small compared to the corresponding values of ΔT_δ and ΔC_δ. Thus, the temperature and the concentration profiles are relatively flat in the bulk solution pool, which have been observed experimentally [13, 23–26]. Equations (29)–(33) lead to

$$\langle w\rangle_c \sim \left[Gr\, Re_m\left(\frac{C_i}{C_0}\right)\right]^{1/3}\left(\frac{\nu}{L}\right) \tag{34}$$

$$\Delta T_c \sim \langle\theta\rangle_c \sim \frac{\lambda_s}{C_p}\left[Gr\, Re_m^{-2}\left(\frac{C_i}{C_0}\right)\right]^{-1/3} \tag{35}$$

$$\Delta C_c \sim \langle\phi\rangle_c - \left[Gr\, Re_m^{-2}\left(\frac{C_i}{C_0}\right)^{-2}\right]^{-1/3} C_0. \tag{36}$$

From equations (35) and (36), we may construct the far-field temperature and concentration profiles, $\bar{T}_c$ and $\bar{C}_c$, respectively, in the turbulent core region as follows:

$$\bar{T}_c = T_0 - \frac{\lambda_s}{C_p}\left[Gr\, Re_m^{-2}\left(\frac{C_i}{C_0}\right)\right]^{-1/3} g_1(\xi) \tag{37}$$

and

$$\bar{C}_c = C_0 - \left[Gr\, Re_m^{-2}\left(\frac{C_i}{C_0}\right)^{-2}\right]^{-1/3} C_0 g_2(\xi) \tag{38}$$

where g_1 and g_2 are unknown functions of ξ to be determined in the course of analysis and $\xi = z/L$ is the turbulent core coordinate. Since molecular transport is not important in this flow region, both g_1 and g_2 are independent of Pr and Sc.

3.3. *Matching of the boundary layer and the turbulent core solutions*

The matching of the near-field and the far-field temperature and concentration profiles in the domain of overlap requires that $\bar{T}_\delta\ (\eta\to\infty) = \bar{T}_c\ (\xi\to 0)$ and $\bar{C}_\delta\ (\eta\to\infty) = \bar{C}_c\ (\xi\to 0)$. From equations (27), (28), (37), and (38), we have

$$\lim_{\eta\to\infty} T_i + \frac{\lambda_s}{C_p} Pr\left[Gr\, Re_m^{-3}\, Sc^2\left(\frac{C_i}{C_0}\right)\right]^{-1/4} f_1(\eta)$$

$$= \lim_{\xi\to 0} T_0 - \frac{\lambda_s}{C_p}\left[Gr\, Re_m^{-2}\left(\frac{C_i}{C_0}\right)\right]^{-1/3} g_1(\xi) \tag{39}$$

and

$$\lim_{\eta\to\infty} C_i + \left[Gr\, Re_m^{-3}\, Sc^{-2}\left(\frac{C_i}{C_0}\right)^{-3}\right]^{-1/4} C_0 f_2(\eta)$$

$$= \lim_{\xi\to 0} C_0 - \left[Gr\, Re_m^{-2}\left(\frac{C_i}{C_0}\right)^{-2}\right]^{-1/3} C_0 g_2(\xi). \tag{40}$$

Differentiating both sides of equations (39) and (40) with respect to z, we yield

$$Pr\, Sc^{-2/3}\frac{\partial f_1}{\partial\eta}(\eta\to\infty) = -\left(\frac{\delta}{L}\right)^{4/3}\frac{\partial g_1}{\partial\xi}(\xi\to 0) \tag{41}$$

and

$$Sc^{1/3}\frac{\partial f_2}{\partial\eta}(\eta\to\infty) = -\left(\frac{\delta}{L}\right)^{4/3}\frac{\partial g_2}{\partial\xi}(\xi\to 0) \tag{42}$$

where equation (24) has been employed in deriving the above equations. Since $\delta/L = (z/L)/(z/\delta) = \xi/\eta$, it follows that

$$\lim_{\eta\to\infty} Pr\, Sc^{-2/3}\eta^{4/3}\frac{\partial f_1}{\partial\eta} = \lim_{\xi\to 0} -\xi^{4/3}\frac{\partial g_1}{\partial\xi} = A_0/3 \tag{43}$$

and

$$\lim_{\eta\to\infty} Sc^{1/3}\eta^{4/3}\frac{\partial f_2}{\partial\eta} = \lim_{\xi\to 0} -\xi^{4/3}\frac{\partial g_2}{\partial\xi} = B_0/3 \tag{44}$$

where A_0 and B_0 are constants, independent of η and ξ. Integration of the above equations leads to

$$f_1 = -A_0\, Pr^{-1}\, Sc^{2/3}\eta^{-1/3} + A_1 \quad \text{for} \quad \eta\to\infty \tag{45a}$$

$$g_1 = A_0\xi^{-1/3} + A_2 \quad \text{for} \quad \xi\to\infty \tag{45b}$$

and

$$f_2 = -B_0 Sc^{-1/3}\eta^{-1/3} + B_1 \quad \text{for} \quad \eta \to \infty \tag{46a}$$

$$g_2 = B_0\xi^{-1/3} + B_2 \quad \text{for} \quad \xi \to 0 \tag{46b}$$

where A_1, A_2, B_1, and B_2 are constants of integration. Note from the properties of f_1, f_2, g_1, and g_2 that A_1 and B_1 are functions of Pr and Sc whereas A_2 and B_2 are independent of Pr and Sc. The fact that (f_1, g_1) and (f_2, g_2) are of the same form is evidently due to the similarity between the turbulent heat and mass transport processes. Substituting equations (45) and (46) into equations (39) and (40), respectively, we obtain

$$T_i + \frac{\lambda_s}{C_p} Pr\left[Gr\, Re_m^{-3}\, Sc^2\left(\frac{C_i}{C_0}\right)\right]^{-1/4} A_1 = T_0 - \frac{\lambda_s}{C_p}\left[Gr\, Re_m^{-2}\left(\frac{C_i}{C_0}\right)\right]^{-1/3} A_2 \tag{47}$$

and

$$C_i + \left[Gr\, Re_m^{-3}\, Sc^{-2}\left(\frac{C_i}{C_0}\right)^{-3}\right]^{-1/4} C_0 B_1 = C_0 - \left[Gr\, Re_m^{-2}\left(\frac{C_i}{C_0}\right)^{-2}\right]^{-1/3} C_0 B_2 \tag{48}$$

where the terms involving A_0 and B_0, respectively, have been eliminated from the above equations using the expression for δ/L as given by equation (24).

Since A_1 and B_1 are functions of Pr and Sc, we may absorb the term $Pr\, Sc^{-1/2}$ on the left-hand side of equation (47) in A_1 and the term $Sc^{1/2}$ on the left-hand side of equation (48) in B_1. After rearrangement, equations (47) and (48) become

$$\frac{C_p(T_0 - T_i)}{\lambda_s} = \left[Gr\, Re_m^{-3}\left(\frac{C_i}{C_0}\right)\right]^{-1/4} \times \left\{A_1 + A_2\left[Gr\, Re_m\left(\frac{C_i}{C_0}\right)\right]^{-1/12}\right\} \tag{49}$$

and

$$1 - \frac{C_i}{C_0} = \left[Gr\, Re_m^{-3}\left(\frac{C_i}{C_0}\right)^{-3}\right]^{-1/4} \times \left\{B_1 + B_2\left[Gr\, Re_m\left(\frac{C_i}{C_0}\right)\right]^{-1/12}\right\}. \tag{50}$$

From equation (14b) together with the relation, $(T_{mp} - T_d) = mC_0$, we have

$$\frac{C_p(T_0 - T_i)}{\lambda_s} = \frac{C_p}{\lambda_s}\left[(T_0 - T_{mp}) + \frac{C_i}{C_0}(T_{mp} - T_d)\right] = Ste + Ste_d\left(\frac{C_i}{C_0}\right). \tag{51}$$

Equation (49) may now be written as

$$1 + \frac{Ste_d}{Ste}\left(\frac{C_i}{C_0}\right) = Ste^{-1}\left[Gr\, Re_m^{-3}\left(\frac{C_i}{C_0}\right)\right]^{-1/4} \times \left\{A_1 + A_2\left[Gr\, Re_m\left(\frac{C_i}{C_0}\right)\right]^{-1/12}\right\}. \tag{52}$$

For given values of Pr and Sc, equations (50) and (52) completely describe the dependencies of (C_i/C_0) and Re_m on Gr, Ste, and Ste_d. Note that A_2 and B_2 are true constants, independent of Pr and Sc, although A_1 and B_1 are strong functions of Pr and Sc.

3.4. *Melting rate correlations*

For moderate values of Pr and Sc, we may expect A_1, A_2 and B_1, B_2 to be of the same order of magnitude. At very high Grashof numbers, the term $[Gr\, Re_m(C_i/C_0)]^{-1/12}$ may be neglected from equations (50) and (52). This gives

$$1 - \frac{C_i}{C_0} = B_1\left[Gr\, Re_m^{-3}\left(\frac{C_i}{C_0}\right)^{-3}\right]^{-1/4} \tag{53}$$

and

$$1 + \frac{Ste_d}{Ste}\left(\frac{C_i}{C_0}\right) = A_1\, Ste^{-1}\left[Gr\, Re_m^{-3}\left(\frac{C_i}{C_0}\right)\right]^{-1/4}. \tag{54}$$

Solving for (C_i/C_0) and Re_m, we have

$$\frac{C_i}{C_0} = \frac{\left[\left(1 + \frac{B_1}{A_1}Ste\right)^2 + 4\frac{B_1}{A_1}Ste_d\right]^{1/2} - \left(1 + \frac{B_1}{A_1}Ste\right)}{2\frac{B_1}{A_1}Ste_d} \tag{55}$$

and

$$Re_m = \frac{(1 - C_i/C_0)^{4/3}}{B_1^{4/3}(C_i/C_0)}\, Gr^{1/3}. \tag{56}$$

The above expressions for (C_i/C_0) and Re_m are exact only if $Gr \to \infty$. However, if Gr is not sufficiently large, higher-order approximations are required. These can be obtained using equations (55) and (56) to get

$$\frac{C_i}{C_0} = \frac{\left[\left(Z + \frac{B_1}{A_1}Ste\right)^2 + 4Z\frac{B_1}{A_1}Ste_d\right]^{1/2} - \left(Z + \frac{B_1}{A_1}Ste\right)}{2\frac{B_1}{A_1}Ste_d} \tag{57}$$

and

$$Re_m = \frac{(1 - C_i/C_0)^{4/3}}{B_1^{4/3}(C_i/C_0)}\left(1 + \frac{B_2}{B_1}Y\right)^{-4/3} Gr^{1/3} \tag{58}$$

where the higher-order quantities Y and Z are given by

$$Y = \left[Gr\, Re\left(\frac{C_i}{C_0}\right)\right]^{-1/12} = \left\{ \frac{2\frac{B_1}{A_1} Ste_d}{\frac{B_1}{Gr}\left[2\frac{B_1}{A_1} Ste_d + \left(1 + \frac{B_1}{A_1} Ste\right) - \left[\left(1 + \frac{B_1}{A_1} Ste\right)^2 + 4\frac{B_1}{A_1} Ste_d\right]^{1/2}\right]} \right\}^{1/9} \tag{59}$$

and

$$Z = \frac{1 + \frac{A_2}{A_1} Y}{1 + \frac{B_2}{B_1} Y}. \tag{60}$$

With the above equations, it is possible to determine how (C_i/C_0) and Re_m deviate from their asymptotic behavior (as described by equations (55) and (56)) for the case when Gr is not sufficiently large.

4. RESULTS AND DISCUSSION

We have identified five important parameters that control the dimensionless melting rate of the Reynolds number, Re_m. These parameters are the Grashof number, Gr, the external Stefan number based on the liquid superheat, Ste, the internal Stefan number based on the freezing-point depression, Ste_d, the Prandtl number, Pr, and the Schmidt number, Sc. Since the present analysis has been restricted to moderate values of Pr and Sc, the exact dependence of Re_m on Pr and Sc cannot be determined. Rather, these material-property effects are represented through the terms involving A_1 and B_1. For given pool–substrate material pairs, however, A_1 and B_1 are constants. Thus, we may focus only on the separate effects of Gr, Ste, and Ste_d. These are given implicitly by equations (50) and (52), and explicitly by equations (56) and (58).

Figure 1 shows the variation of the dimensionless interface concentration (C_i/C_0) with Ste and Ste_d. In constructing this figure, we have assumed $A_2/A_1 = B_2/B_1$ in equations (45) and (46) based on the argument that the processes of turbulent heat and mass transport are similar. This argument is deemed appropriate because turbulence is a flow property that acts to transport quantities equally. It follows that equation (57) may be reduced to equation (55). Hence, (C_i/C_0) is a function of $(B_1/A_1)Ste$ and $(B_1/A_1)Ste_d$ only and is independent of Gr. This is true as long as the flow is fully turbulent or equivalently, the value of Gr is very large. From Fig. 1, it is evident that (C_i/C_0) is a monotonically decreasing function of Ste_d and Ste. For a given value of $(B_1/A_1)Ste_d$, (C_i/C_0) approaches asymptotically to zero as $Ste \to \infty$ whereas it approaches a constant value less than unity as $Ste \to 0$.

The effects of Gr, Ste, and Ste_d on the dimensionless melting rate, Re_m are displayed in Fig. 2, where the quantity, $B_1^{4/3} Re_m/Gr^{1/3}$, is plotted against $(B_1/A_1)Ste$ on a log–log scale with $(B_1/A_1)Ste_d$ as a parameter. The results for two different values of Gr, i.e. $Gr \to \infty$ and $Gr = 1 \times 10^9$, are shown in the figure. It is evident from equations (56) and (58) that Re_m would vary approximately according to the 1/3-power of Gr at large Grashof numbers. This is demonstrated in Fig. 2. For all values of Ste and Ste_d, the quantity, $Re_m/Gr^{1/3}$, is indeed a weak function of Gr. Thus, to the first approximation, we may expect the melting rate to vary with the pool-to-substrate density ratio according to $V \sim (\Delta\rho/\rho_0)^{1/3}$. This result is consistent with the experimental observations of Fang *et al.* [25] and Epstein and Grolmes [26]. For a given value of Gr, Re_m is a monotonically increasing function of Ste and Ste_d. In fact, as $Ste \to \infty$, Re_m is a linear function of Ste for all values of Ste_d. Thus, we have $V \sim \Delta T$ for $Ste \gg 1$ (high temperature region). This linear dependence of the melting rate on the pool-to-substrate temperature difference has been observed by Eck and Werle [24] and Epstein and Grolmes [26]. However, except for the limiting case of $Ste_d = 0$, the value of Re_m does not approach zero as $Ste \to 0$. Rather, Re_m approaches a positive, non-zero, constant value at small Ste. From Fig. 2, it is evident that for $Ste < 0.1Ste_d$, Re_m is almost independent of Ste as long as both Ste and Ste_d are non-zero, positive quantities. Under this situation, the melting rate is insensitive to the variation of the pool-to-substrate temperature difference. This explains qualitatively the experimental observations of Catton *et al.* [23] and Fang *et al.* [25].

To further explore the effects of Ste and Ste_d on the dimensionless melting rate in the small-Ste regime (low-temperature regime), the quantity, $B^{4/3} Re_m/Gr^{1/3}$ is plotted against $(B_1/A_1)Ste$ on a regular scale with $(B_1/A_1)Ste_d$ as a parameter (Fig. 3). Again, two different values of Gr, i.e. $Gr \to \infty$ and $Gr = 1 \times 10^9$, are shown in the figure. For given values of Gr and Ste_d, Re_m is a non-zero positive quantity provided that $Ste > -Ste_d$. Thus melting of the solid substrate would occur even though the bulk pool temperature, T_0, is below the normal melting point of the solid. Mathematically, we have $V > 0$ for

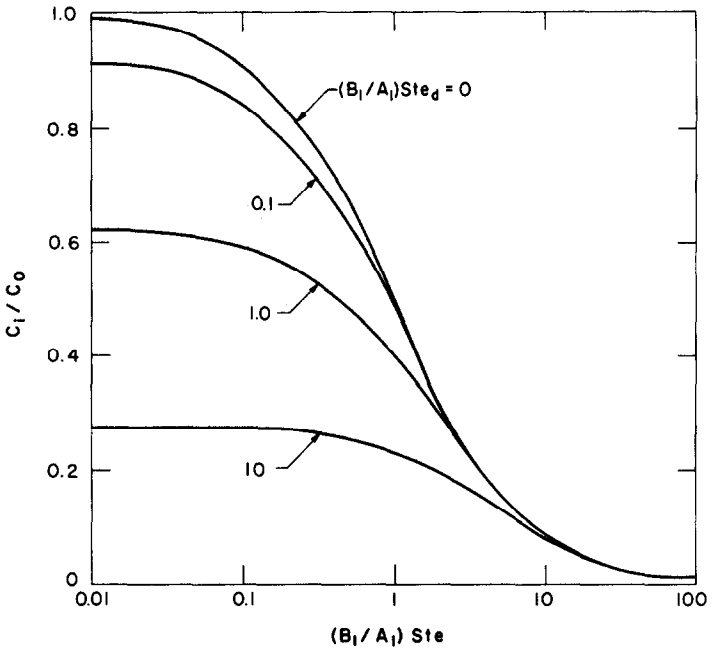

FIG. 1. Variation of the dimensionless interface concentration with the external and internal Stefan numbers.

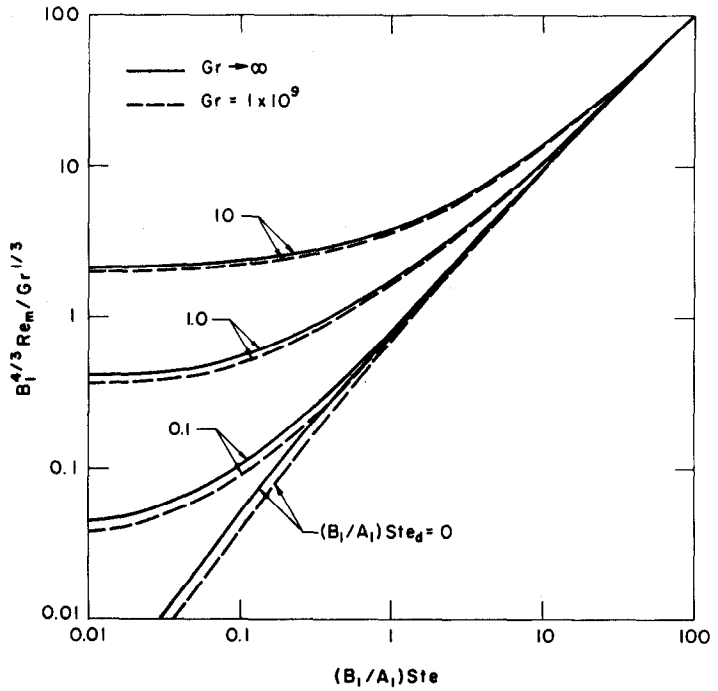

FIG. 2. Effects of the Grashof number, the external Stefan number, and the internal Stefan number on the dimensionless melting rate.

$T_0 > T_d$. Inspection of Fig. 3 indicates that the various curves for a given Gr (either those represented by the solid lines or those by the dashed lines) are very similar. This implies that we may be able to combine these curves into one by plotting the quantity, $B_1^{4/3}\ Re_m/Gr^{1/3}$, against $(B_1/A_1)\ (Ste + Ste_d)$. This is shown in Fig. 4. It is evident that for small values of $(Ste + Ste_d)$, we have

$$B_1^{4/3}\, Re_m/Gr^{1/3} = 1.09\left[\frac{B_1}{A_1}(Ste + Ste_d)\right]^{1.33}. \quad (61)$$

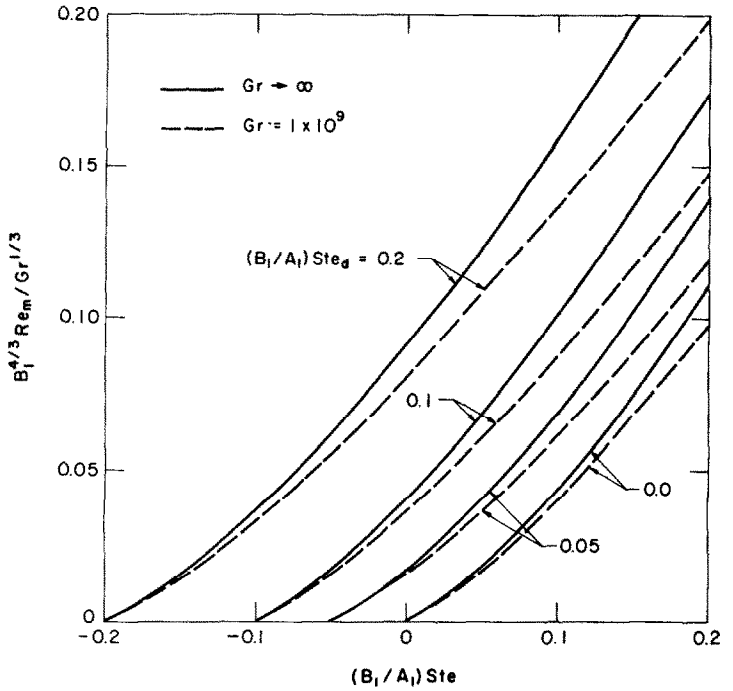

FIG. 3. Variation of the dimensionless melting rate with the external and the internal Stefan numbers in the low-temperature regime.

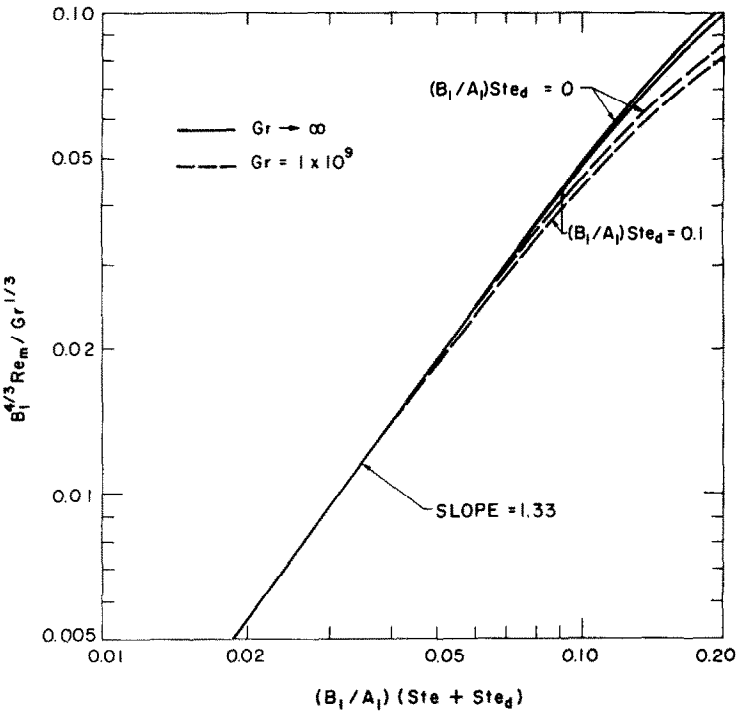

FIG. 4. The combined effect of the external and the internal Stefan numbers on the dimensionless melting rate in the low-temperature regime.

Significant deviations from the above equation occurs only when $(B_l/A_l)\,(Ste + Ste_d) > 0.1$. In terms of the original physical quantities, we have $V \sim (\Delta T + \Delta T_d)^{1.33}$ in the low-temperature regime. As $\Delta T \to 0$, the melting rate approaches a constant value proportional to $\Delta T_d^{1.33}$. So far, this important melting regime has not been studied in previous work [13, 23–26].

It is of interest to estimate how large the value of Gr is required in order that the asymptotic behavior of Re_m as given by equation (60) is rigorously satisfied. Also, it is important to determine how Re_m deviates from its asymptotic behavior at lower Grashof numbers. In Fig. 5, the ratio, $Re_m/Re_m\,(Gr \to \infty)$, is plotted against Gr/B_1 with $(B_1/A_1)Ste$ and $(B_1/A_1)Ste_d$ as parameters. It is evident that Re_m would achieve its asymptotic value with less than 1% error only if $Gr/B_1 > 1 \times 10^{20}$. Below this Grashof number, we have $Re_m < Re_m\,(Gr \to \infty)$. If we correlate the Re_m–Gr relation by a simple power-law, i.e. $Re_m \sim Gr^n$, the index n would be less than 1/3 for $Gr/B_1 < 1 \times 10^{20}$. The deviation is larger at lower values of Gr, Ste, and Ste_d. Nevertheless, for $Gr/B_1 > 1 \times 10^9$ and $(B_1/A_1) \times (Ste + Ste_d) > 0.1$, it can be shown that Re_m can be approximated by its asymptotic value with less than 20%. In most cases, these requirements for Gr, Ste, and Ste_d are usually met, and hence we may determine the melting rate using equation (56) as a first approximation.

The validity of the present model requires the quantity $[Gr\,Re_m(C_i/C_0)]^{1/3}$, to be much larger than one. It is, therefore, necessary to determine the ranges of Gr, Ste, and Ste_d for which this condition is met. From equations (55) and (56), we have

$$\left[Gr\,Re_m\left(\frac{C_i}{C_0}\right)\right]^{1/3} = \left\{\frac{Gr}{B_1}\frac{\left[2\frac{B_1}{A_1}Ste_d + \left(1+\frac{B_1}{A_1}Ste\right)\right] - \left[\left(1+\frac{B_1}{A_1}Ste\right)^2 + 4\frac{B_1}{A_1}Ste_d\right]^{1/2}}{2\frac{B_1}{A_1}Ste_d}\right\}^{4/9} \tag{62}$$

If we arbitrarily set $[Gr/Re_m(C_i/C_0)]^{1/3} > 100$ to be the criterion, this requires

$$\frac{Gr}{B_1} > \frac{6.32 \times 10^4 \frac{B_1}{A_1}Ste_d}{2\frac{B_1}{A_1}Ste_d + \left(1+\frac{B_1}{A_1}Ste\right) - \left[\left(1+\frac{B_1}{A_1}Ste\right)^2 + 4\frac{B_1}{A_1}Ste_d\right]^{1/2}}. \tag{63}$$

In most free convection melting problems, we may expect $A_1 \sim B_1$ and $(Ste + Ste_d) > 0.03$. Under these conditions, the above inequality is satisfied as long as $Gr/B_1 > 1 \times 10^6$. Note that A_1 and B_1 are functions of Pr and Sc and must be determined for each pool-to-substrate material pair.

To further examine the validity of the present model, comparison of the predicted results are made with the experimental data of Fang *et al.* [25] and Epstein and Grolmes [26]. Figure 6 presents the measured and the predicted variations of the melting rate, V_s, with the pool-to-substrate density ratio, $\Delta\rho/\rho_0$, for the case of ice melting in KI solution. The data of Epstein and Grolmes [26] were taken at $\Delta T = 24°C$, corresponding to $Ste = 0.3$, with a pool depth of $L = 0.14$ m. The data of Fang *et al.* [25], on the other hand, were taken at $\Delta T = 15°C$, corresponding to $Ste = 0.19$, with a pool depth of $L = 0.123$ m. Equations (55) and (56) are employed along with equation (15) to determine the value of V_s. The physical properties used in the calculations are $C_p = 4.18\,\mathrm{kJ\,kg^{-1}\,K^{-1}}$, $\lambda_s = 330\,\mathrm{kJ\,kg^{-1}}$, $\rho_s = 0.92 \times 10^3\,\mathrm{kg\,m^{-3}}$, and $\nu = 1.3 \times 10^6\,\mathrm{m^2\,s^{-1}}$. Since $Ste_d < 0.1$ over the experimental conditions explored in refs. [25, 26], we have

$$\left(1 + \frac{B_1}{A_1}Ste\right) \gg \frac{B_1}{A_1}Ste_d. \tag{64}$$

Equations (55) and (56) may be reduced to

$$\frac{C_i}{C_0} = \left(1 + \frac{B_1}{A_1}Ste\right)^{-1}$$

and (65)

$$Re_m = \frac{\left(\frac{B_1}{A_1}Ste\right)^{4/3}}{B_1^{4/3}}\left(1 + \frac{B_1}{A_1}Ste\right)^{-1/3} Gr^{1/3}.$$

Using two typical data points of Epstein and Grolmes [26], i.e. $V_s = 0.052$ and $0.066\,\mathrm{mm\,s^{-1}}$ for $(\Delta\rho/\rho_0) = 0.1$ and 0.2, respectively, the values of A_1 and B_1 are determined to be $A_1 = 15.5$ and $B_1 = 31.9$. Note from equation (65) that the melting rate is independent of the pool depth, L, since $Re_m \sim Gr^{1/3}$. Based on these values of A_1 and B_1, the predicted variations of V_s with $(\Delta\rho/\rho_0)$ are shown in Fig. 6 for the case of $Ste = 0.19$ and the case of $Ste = 0.3$. Evidently, the present results compare favorably with both sets of data. Using the same values of A_1 and B_1, the predicted variation of V_s with the pool-to-substrate temperature difference, ΔT, is shown in Fig. 7 for the case of $(\Delta\rho/\rho_0) = 0.38$, corresponding to $Gr = 8 \times 10^8$. Also shown in the figure are the

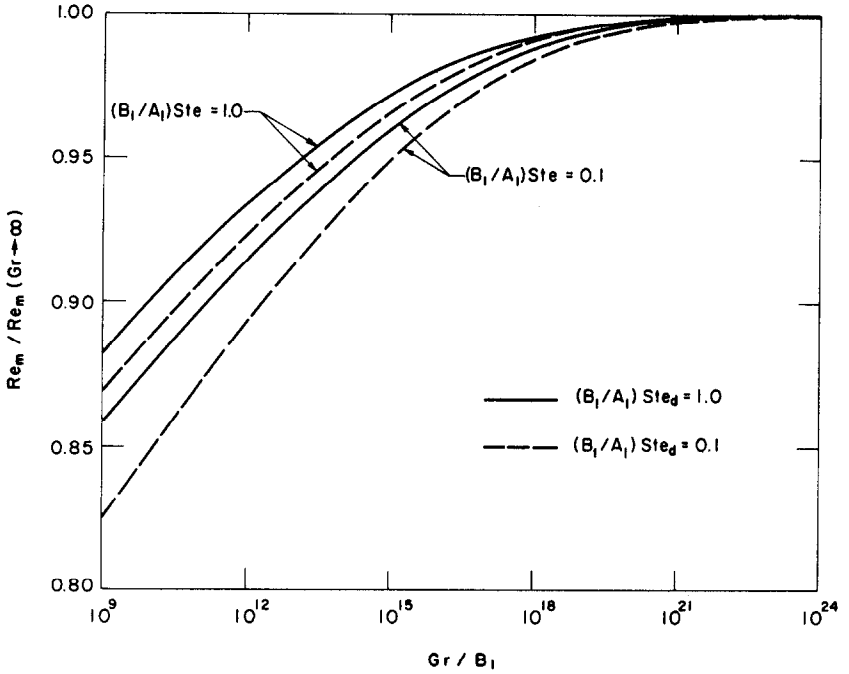

FIG. 5. Deviation of the dimensionless melting rate from the asymptotic behavior at different Grashof numbers.

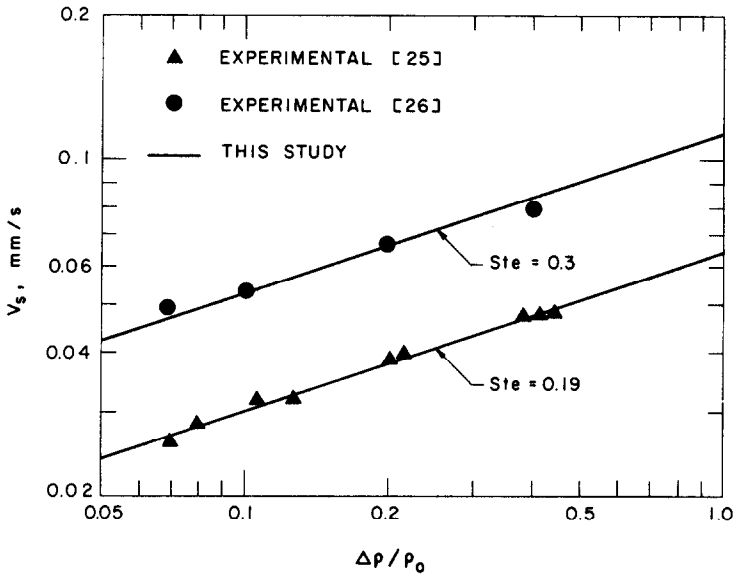

FIG. 6. The measured and the predicted variations of the melting rate with the pool-to-substrate density ratio at two different external Stefan numbers for the case of ice melting in KI solution.

experimental data of Epstein and Grolmes [26]. Again, there is good agreement between the measured data and the predicted results. Within the range of ΔT displayed in the figure, the melting rate can be correlated to the temperature difference as $V \sim \Delta T^{1.2}$.

5. CONCLUDING REMARKS

We have identified the effects of *Gr*, *Ste*, and Ste_d on the dimensionless melting rate, Re_m. In particular, we have shown that at large values of *Gr*, the melting rate is approximately proportional to the pool-to-substrate density ratio raised to the 1/3 power, i.e. $V_s \sim (\Delta\rho/\rho_0)^{1/3}$. However, at lower values of *Gr*, considerable deviation from the 1/3-power-law behavior may occur with $V_s \sim (\Delta\rho/\rho_0)^n$ where n is less than 1/3. We have also demonstrated that in the high-temperature regime, corresponding to large values of *Ste*, the melting rate is a linear function of the pool-to-substrate temperature difference, i.e. $V_s \sim \Delta T$. This is consistent with the experimental observations of Eck and Werle [24] and Epstein and Grolmes [26].

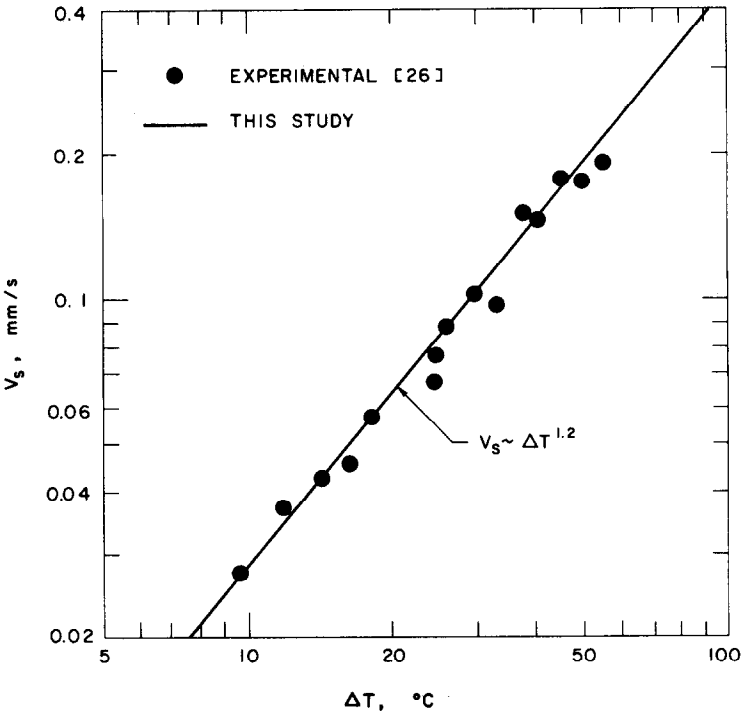

FIG. 7. The measured and the predicted variations of the melting rate with the pool-to-substrate temperature difference at a density ratio of 0.38 for the case of ice melting in $ZnBr_2$ solution.

On the other hand, in the low-temperature regime, corresponding to small values of $(Ste + Ste_d)$, the melting rate is given by $V_s \sim (Ste + Ste_d)^{1.33}$. As $Ste \to 0$, V_s approaches a non-zero, positive, constant value proportional to $Ste_d^{1.33}$. Thus, the melting rate is quite insensitive to the variation in the pool-to-substrate temperature difference for small values of *Ste*. This explains the experimental observations of Catton *et al.* [23] and Fang *et al.* [25]. Additional experimental data, however, are needed to confirm the melting rate behavior in the low-temperature regime, especially regarding the effect of freezing-point depression, i.e. the parameter Ste_d.

In the present analysis, the effect of *Pr* and *Sc* are implicitly represented by the terms involving A_1 and B_1. The functional forms of A_1 and B_1 can be determined empirically by setting $A_1 = a\,Pr^{m_1}\,Sc^{m_2}$ and $B_1 = b\,Pr^{n_1}\,Sc^{n_2}$. Unfortunately, there are not sufficient data available for us to determine the coefficients a and b and the indices m_1, m_2, n_1 and n_2. Additional experimental studies covering a wide range of pool–substrate material pairs with selected values of $(\Delta\rho/\rho_0)$ and ΔT are required to determine the dependence of A_1 and B_1 on *Pr* and *Sc*. It should be noted that in some cases, the viscosity of the convecting fluid may vary by several orders of magnitude across the pool. As a result, the turbulent core properties can be quite different from the constant-viscosity case [27]. The effect of property variation needs to be further examined.

Acknowledgements—This work was supported by the PSU Research Initiation Grant No. 415-51-1001 W (1986/87).

REFERENCES

1. M. Epstein and F. B. Cheung, Complex freezing–melting interfaces in fluid flow, *A. Rev. Fluid Mech.* **15**, 293–310 (1983).
2. F. B. Cheung and M. Epstein, Solidification and melting in fluid flow, *Adv. Transp. Processes* **3**, 35–117 (1984).
3. M. E. Glicksman, S. R. Corriell and G. B. McFadden, Interactions of flows with the crystal–melt interface, *A. Rev. Fluid Mech.* **18**, 307–335 (1986).
4. E. M. Sparrow, S. V. Patankar and S. Ramadhyeni, Analysis of melting in the presence of natural convection in the melt region, *J. Heat Transfer* **99**, 520–526 (1977).
5. E. M. Sparrow, R. R. Schmidt and J. W. Ramsey, Experiments on the role of natural convection in the melting of solids, *J. Heat Transfer* **100**, 11–16 (1978).
6. J. W. Ramsey and E. M. Sparrow, Melting and natural convection during a vertical embedded heater, *J. Heat Transfer* **100**, 368–370 (1978).
7. R. J. Goldstein and J. W. Ramsey, Heat transfer to a melting solid with application to thermal energy storage systems. *Studies in Heat Transfer*, pp. 199–208. Hemisphere, Washington, D.C. (1978).
8. A. G. Bathelt, R. Viskanta and W. Leidenfrost, An experimental investigation of natural convection in the melted region around a heated horizontal cylinder, *J. Fluid Mech.* **90**, 227–239 (1979).

9. A. G. Bathelt and R. Viskanta, Heat transfer at the solid–liquid interface during melting from a horizontal cylinder, *Int. J. Heat Mass Transfer* **23**, 1493–1503 (1980).
10. N. W. Hale, Jr. and R. Viskanta, Solid–liquid phase change heat transfer and interface motion in materials cooled or heated from above or below, *Int. J. Heat Mass Transfer* **23**, 283–292 (1980).
11. H. E. Huppert and R. S. J. Sparks, Double-diffusive convection due to crystallization in magmas, *A. Rev. Earth Planet. Sci.* **12**, 11–37 (1984).
12. J. S. Turner, Multicomponent convection, *A. Rev. Fluid Mech.* **II**, 11–44 (1985).
13. R. Farhadieh and L. Baker, Jr., Heat transfer phenomenology of a hydrodynamically unstable melting system, *J. Heat Transfer* **100**, 305–310 (1978).
14. E. M. Sparrow, R. B. Husar and R. J. Goldstein, Observations and other characteristics of thermals, *J. Fluid Mech.* **41**, 739–780 (1970).
15. K. Onat and V. Grigull, The onset of convection in a horizontal fluid layer heated from below, *Warme- u. Stoffugertr.* **3**, 103–113 (1970).
16. T. Y. Chu and R. J. Goldstein, Turbulent convection in a horizontal layer of water, *J. Fluid Mech.* **60**, 141–159 (1973).
17. A. M. Garon and R. J. Goldstein, Velocity and heat transfer measurement in thermal convection, *Physics Fluids* **16**, 1818–1825 (1973).
18. D. C. Threlfall, Free convection in low-temperature gaseous helium, *J. Fluid Mech.* **67**, 17–28 (1975).
19. F. A. Kulacki and M. E. Nagle, Natural convection in a horizontal fluid layer with volumetric energy sources, *J. Heat Transfer* **91**, 204–211 (1975).
20. F. A. Kulacki and A. A. Emara, Steady and transient thermal convection in a fluid layer with uniform volumetric energy sources, *J. Fluid Mech.* **83**, 375–395 (1977).
21. Y. Kikuchi, T. Kawasaki and T. Shioyama, Thermal convection in a horizontal fluid layer heated internally and from below, *Int. J. Heat Mass Transfer* **25**, 363–370 (1982).
22. Y. Kikuchi, T. Shioyama and Z. Kawara, Turbulent heat transport in a horizontal fluid layer heated internally and from below, *Int. J. Heat Mass Transfer* **29**, 451–461 (1986).
23. I. Catton, W. A. Brinsfield and S. M. Ghiaasiaan, Heat transfer from a heated pool to a melting miscible substrate, *J. Heat Transfer* **105**, 447–543 (1983).
24. G. Eck and H. Werle, Experimental studies of penetration of a heated liquid pool into a melting miscible substrate, *Nucl. Tech.* **64**, 275–289 (1984).
25. L. J. Fang, F. B. Cheung, J. H. Linehan and D. R. Pederson, An experimental study of natural convection melting of ice in salt solutions, ASME Winter Annual Meeting, New Orleans, Paper No. 84-WA/HT-55 (1984).
26. M. Epstein and M. A. Grolmes, Natural convection characteristics of pool penetration into a melting miscible substrate, *J. Heat Transfer* **108**, 190–197 (1986).
27. F. M. Richter, H. Nataf and S. F. Daly, Heat transfer and horizontally averaged temperature of convection with large viscosity variations, *J. Fluid Mech.* **129**, 173–192 (1983).

CONVECTION NATURELLE DE CHALEUR ET DE MASSE PENDANT LA PENETRATION DANS UN SUBSTRAT MISCIBLE EN FUSION

Résumé—On étudie théoriquement le mécanisme de fusion libre d'une plaque solide surmontée d'une masse de liquide chaud. Le solide, lorsqu' il fond, devient plus léger et miscible dans l'autre liquide. Des approximations des équations du mouvement selon Boussinesq sont faites pour déterminer le comportement des champs de température et de concentration dans deux régions différentes : la région de couche limite à l'interface et la région turbulente dans la masse liquide. Par confrontation de la solution dans la couche limite et de celle dans le noyau turbulent, dans la zone de recouvrement, on obtient la dépendance de la vitesse à différents paramètres, dont le nombre de Grashof basé sur le rapport de densité bain-substrat, le nombre de Stefan externe basé sur la différence de température bain-substrat, et le nombre de Stefan interne basé sur la dépression du point de congélation. Une comparaison entre la théorie et les données expérimentales existantes donne satisfaction.

WÄRME- UND STOFFÜBERGANG BEIM SCHMELZEN EINES MISCHBAREN STOFFES IN EINEM MIT FLÜSSIGKEIT GEFÜLLTEN BEHÄLTER

Zusammenfassung—Der Schmelzvorgang bei freier Konvektion an einer festen Platte in einer heißen Flüssigkeit wird theoretisch untersucht. Der geschmolzene Feststoff besitzt eine geringere Dichte als die umgebende Flüssigkeit und ist mit ihr mischbar. Um das Temperatur- und Strömungsfeld für zwei verschiedene Bereiche zu ermitteln, werden systematische mathematische Näherungen der Bewegungsgleichung von Boussinesq benutzt. Die beiden Bereiche sind die Grenzschicht an der Schmelzfront und die turbulente Kernströmung in der umgebenden Flüssigkeit. Die Abhängigkeit der Schmelzrate von verschiedenen Parametern wird durch Anpassung der Lösungen für die beiden Bereiche Grenzschicht und Kernbereich in der Übergangsregion zwischen beiden erhalten. Diese Parameter sind die Grashof-Zahl (gebildet mit dem Dichteunterschied zwischen schmelzender Substanz und umgebender Flüssigkeit), die äußere Stefan-Zahl (gebildet mit der Temperaturdifferenz zwischen schmelzender Substanz und umgebender Flüssigkeit) und die innere Stefan-Zahl (gebildet mit der Schmelzpunkterniedrigung). Die vorgestellte Theorie wird mit vorhandenen experimentellen Werten verglichen, die Übereinstimmung ist gut.

СВОБОДНОКОНВЕКТИВНЫЙ ТЕПЛО- И МАССОПЕРЕНОС ПРИ ПОСТУПЛЕНИИ ЖИДКОСТИ В РАСПЛАВЛЯЮЩУЮ ПОДЛОЖКУ В ПРОЦЕССЕ ИХ СМЕШЕНИЯ

Аннотация—Проведено теоретическое изучение свободной конвекции при плавлении твердого слитка в большом объеме горячей жидкости, находящейся над ним. Расплавившаяся фаза легче жидкости и смешивается с ней. Сформулирована система уравнений в приближении Буссинеска с целью определения эволюции изменения полей температуры и концентрации в двух различных областях течения: пограничного слоя на границе плавления и турбулентного ядра в объеме жидкости. Получена зависимость скорости плавления от различных режимных параметров, в том числе числа Грасгофа, в которое входят отношение плотностей окружающей жидкости и подложки, внешнее число Стефана, основанное на разности температур жидкости и подложки, и внутреннее число Стефана, основанное на понижении точки замерзания. Для этого сшивались решения в области пересечения пограничного слоя и турбулентного ядра. При сравнении теории с имеющимися экспериментальными данными найдено их хорошее соответствие.